# Investigating the Bioavailability of Nutrients and Metals From Hydrothermally Active Shallow Seamounts of the Mariana Arc

Elise Herzfeld
hertzy@uw.edu

University of Washington
School of Oceanography

1503 NE Boat Street, Box 357940
Seattle, WA 98195-7940

5 June 2026

## Abstract

Hydrothermal vents have recently been recognized to have an impact on the global inventory of essential trace nutrients due to the enhanced concentrations of metals like iron (Fe) and manganese (Mn) in hydrothermal fluids. Past studies have hypothesized that hydrothermal inputs could influence surface ocean productivity, yet limited studies have displayed a direct connection. In this study, we utilize the shallow seamounts of the Mariana Arc to investigate (a) how the abnormally shallow nature of these vent sites may facilitate the transport of metal-rich hydrothermal fluids to the euphotic zone and (b) the potential for these fluids to fuel phytoplankton productivity. In a set of incubation experiments, we added hydrothermal plume waters from the shallow seamounts of NW Rota-1 (470 m) and Esmeralda (225 m) to surface waters and incubated them for 60 hours. We found that the shallowest vent site, Esmeralda, had the greatest water column concentrations of dissolved Fe (15-30 nM), but that the average net growth rate of $0.825 \pm 0.042$ $day^{-1}$ was not statistically different from background stations. This work demonstrated that hydrothermal fluids from seamounts are bioavailable and that shallow seamount venting has the potential to promote surface primary production through chemical and physical nutrient supplementation.



## Plain Language Summary

Underwater volcanoes, otherwise known as seamounts, have hydrothermal vents that release warm, buoyant water that rises and disperses. These warm fluids are often enriched in metals like iron and manganese, which are nutrients that typically limit ocean productivity due to their naturally low concentrations in this region. Generally, in the Mariana Arc, the ocean surface is depleted in nitrate, iron, manganese, and other nutrients, limiting the amount of growth for organisms in the surface waters, particularly phytoplankton. This creates a zone of low total primary production in the subtropical gyres of the global ocean. When a seamount vents and releases metal-rich fluids, there is the potential for the warm fluids to rise into the surface ocean and provide nutrients. We predicted that shallower seamounts, with summits closer to the surface, were more likely to have fluids with high concentrations of metals that could influence phytoplankton growth in surface waters. We found that the shallowest seamount had the highest metal concentrations and stimulated the most phytoplankton growth in shipboard experiments, but there are many more factors that could influence whether this occurs in-situ, such as seamount shape, ocean currents, and level of venting activity.

# Introduction

Hydrothermal vents produce plumes of hot, buoyant water enriched in metals that rise into the water column and disperse. These plumes contain micromolar levels of metals (Tivey, 2007), elevating the typical low nanomolar concentrations of the open Pacific. Even just small amounts of these micronutrients, such as Fe, can be crucial for the growth of phytoplankton, which are the base of the marine food web. When they are present in too low concentrations or absent altogether, they act as limiting nutrients. The open ocean, far from terrestrial and fluvial inputs, is relatively depleted in these key trace nutrients.

Many active vent sites are along hydrothermal ridges, with depths greater than 2,300 m (Beaulieu et al., 2020). These deep vents are known to support unique local benthic ecosystems, but there are limited studies that have explored whether hydrothermal fluids can impact surface waters. In many cases, the plume is too deep to reach the photic zone before it reaches neutral buoyancy and dilutes with surrounding seawater. However, there is some evidence that submarine volcanoes supply micronutrients that impact biological activity in the photic zone. This includes studies from the Southern Ocean (Schine et al., 2021) and at shallow seamounts in the Kermadec Arc (Kleint et al., 2022), where either the vents themselves are shallow enough that the rising plume can reach the euphotic zone, or the local circulation provides a mechanism for the plume to reach surface waters.

Shallow seamounts, especially vents that are within 300 m of the surface, may have a greater impact on surface productivity as the plume has a greater chance of extending into the euphotic zone. In addition to hydrothermal inputs, seamount bathymetry can increase upwelling of deep waters (Ma et al., 2021). These dynamics may further support the rise of the plume and nutrients supplied from depth (Oliveira et al., 2016). In many cases, it has been unclear if hydrothermal fluids reach the euphotic zone and if the metals and nutrients in the fluids are in a chemical form that is accessible, or bioavailable, to surface microbial communities.

The Izu-Bonin-Mariana subduction zone of the western equatorial Pacific is home to an array of seamounts, with evidence of active and prolonged venting in the region. Resing et al. (2009) explored hydrothermalism in this region, finding strong vent and plume signals at 10 submarine volcanoes. This work confirmed that fluids were of hydrothermal origin and used Fe:Mn ratios, $CO_2$, and helium ($^3He$) to unravel geologic source information. Past work prioritized identifying and categorizing hydrothermal venting sites and is often built upon with a foundational determination of hydrothermal fluxes (Buck et al., 2018) and chemical composition (Resing et al., 2009). Due to the abnormally shallow nature of these seamounts, these studies have emphasized that many of the processes in this region cannot be considered the global model of seamount hydrothermalism. These seamounts offer a unique study area to evaluate the impacts of hydrothermalism on surface ocean productivity. Further, the broad nutrient limitation and oligotrophic nature of the region draw interest for deep water supplementation (Ma et al., 2019).

This project sought to answer how the abnormally shallow nature of these vent sites may influence bioavailable hydrothermal fluids reaching the euphotic zone and assess the potential

for these fluids to fuel phytoplankton productivity. We investigated the shallow seamounts of NW Rota-1 (summiting at 470 m depth) and Esmeralda (summiting at 225 m depth) to explore if fluids from shallow (< 300 m) seamount venting impact phytoplankton growth using shipboard incubation experiments. Understanding how and where hydrothermalism can influence primary productivity will better constrain current biogeochemical models representing the ocean Fe cycles (Resing et al., 2015).

# Methods

### Study region and water column sampling

The 2026 Senior Thesis Cruise, TN450, aboard the R/V *Thomas G. Thompson*, sampled along the Mariana Arc in the equatorial western Pacific from 20 March 2026 to 1 April 2026, beginning and ending in Apra, Guam. For this study, the primary area of interest was the southern chain of seamounts, specifically Esmeralda and NW Rota-1. At the summit of each seamount, as well as 10 nautical miles northeast upstream of each summit, a Sea-Bird SBE 911plus CTD (Conductivity, Temperature, and Depth; Seabird Scientific) cast was performed to detect potential plume signals. On the downcast, a light scattering sensor (LSS), an oxidation-reduction-potential (ORP) sensor (Koichi Eh sensor), and a WET Labs C-Star (Seabird Scientific) transmissometer were used to target hydrothermal fluids for sample collection, primarily at the summit stations. A 24 10-L Niskin bottle (Seabird Scientific) rosette was used for water sample collection for nutrient and trace metal analysis.

Trace metal samples were collected on even-numbered Niskin bottles, which had metal springs replaced with Teflon-coated internal springs to reduce metal contamination. Surface trace metal samples were collected with polyethylene tubing lowered to 15 m depth on a braided nylon line connected to a Teflon diaphragm pump (Walden Incorporated). The ship drifted during surface water collection to reduce contamination. All trace metal samples were filtered using a clean 0.2 μm capsule filter (Acropak 200, Pall Corporation).

### Incubation experimental design

A set of incubation experiments was performed at each seamount of interest to test whether hydrothermal fluids were bioavailable to surface phytoplankton communities. These incubations included treatment groups of background, caldera, and plume fluids added to surface water to observe growth and nutrient consumption (Figure 1). Background spike fluids were used as a control treatment of deep water without the influence of hydrothermal fluids but with comparative macronutrient concentrations (nitrate, nitrite, and phosphate). The water used for the background treatment at each seamount was collected 10 nautical miles upstream of each seamount summit. The water was collected at a depth of 200 m following the trace metal water column sample collection procedure outlined earlier. Caldera fluids were collected as close to the bowl-shaped summit depression as possible. Plume fluids were collected in the neutrally buoyant plume. The caldera and plume spike fluids were collected at targeted depths determined by the CTD downcast indicators, specifically low beam transmission on the transmissometer and an

increase in reductive fluids on the Koichi sensor, which were characteristic indicators of reducing, high particle hydrothermal fluids. At Esmeralda, water for the caldera spike fluids was collected at 200 m, and water for the plume treatment at 190 m. At NW Rota-1, water for the caldera treatment was collected at 400 m, and the plume fluids at 393 m depth.

Surface water for each experiment was collected at 15 m depth, above the summit of each seamount. 500 mL of surface water was pumped through a 100 µm mesh filter into polycarbonate bottles that had a capacity of 600 mL. 100 mL of hydrothermal (caldera or spike) or background fluid was added to each bottle with the corresponding treatments for a 1:5 dilution in their respective bottles (Figure 1). Treatments were performed in triplicate, with a fourth bottle prepared to pull initial samples of the same dilution for trace metals, nutrients, and chlorophyll-*a*. The bottles were incubated at 28-30 ºC in a screened, temperature-controlled incubation tank on the rear deck of the ship. The bottles were incubated for 60 hours. At the end of the incubation period, samples for nutrients, unfiltered trace metal samples (hereafter, total dissolvable trace metals), and chlorophyll-*a* were taken from the bottles, in that order. The analysis procedures for the samples are outlined further in the following sections.

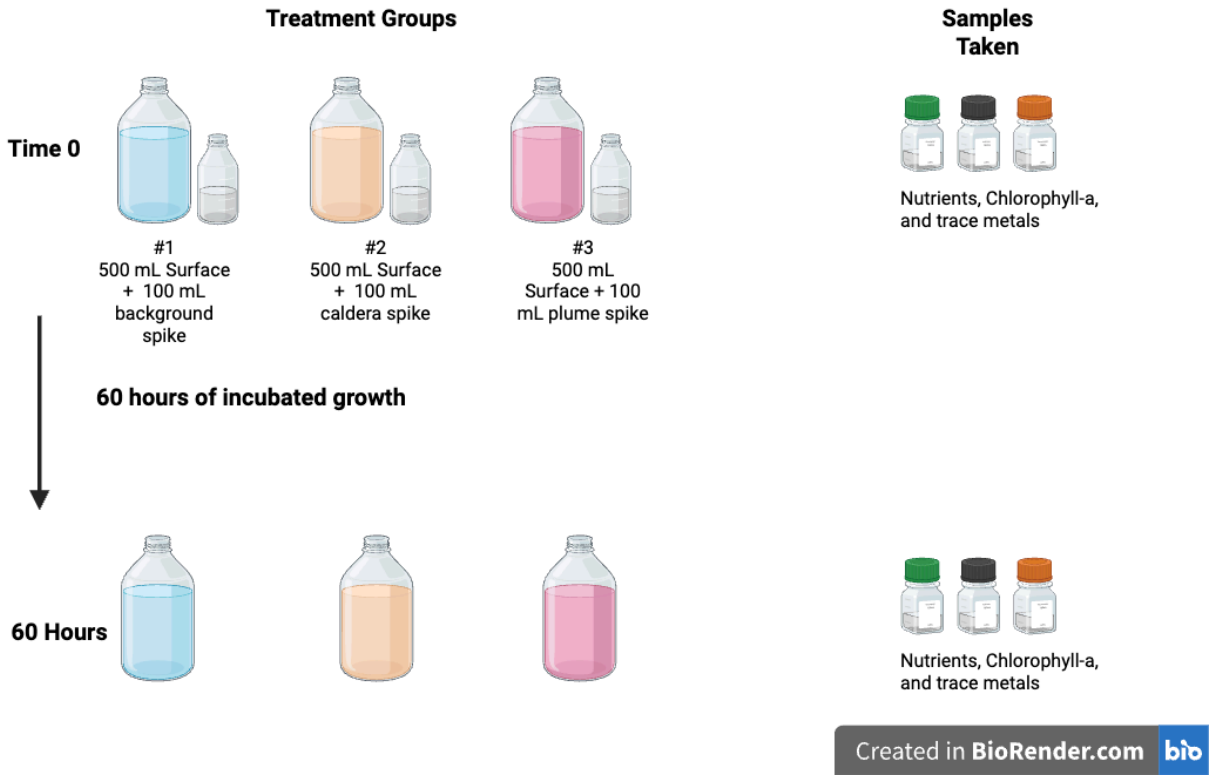


**Figure 1:** Incubation schematic illustrating the treatment groups and sample collection scheme. This study used three treatment groups with either a spike of background or hydrothermal fluids. Incubations were performed in triplicate, with a fourth bottle prepared for initial, time 0, sample

collection. Nutrient, chlorophyll-*a*, and trace metal samples were collected at time 0 and the end of the 60-hour incubation period.

**Trace Metal Analysis**

Filtered and unfiltered trace metal samples were acidified to pH 1.8 (Optima HCl, Fisher Scientific) and stored at room temperature for later lab-based analysis. Samples with high expected metal concentrations, such as those from suspected plumes or seamount summits, were processed by adding 167 µL of the acidified sample to 5 mL of 2% nitric acid (Optima, Fisher Scientific, or distilled). The samples were then analyzed using inductively-coupled plasma mass spectrometry (ICP-MS) on an iCap-RQ ICP-MS (Thermo Scientific). Low concentration samples (< 10 nM) were pre-concentrated before analysis with a seaFAST pico column pre-concentration system (Elemental Scientific Incorporated). Samples were pre-concentrated by a factor of 20, as 10 mL of each filtered sample was pre-concentrated on a column (Nobias-1 resin), followed by elution with 500 µL of 5% nitric acid. The eluted samples were then analyzed on an Element 2 ICP-MS (Thermo Scientific) and quantified using isotope dilution for Fe and a standard addition method for Mn. Concentrations were normalized with an internal standard and then quantified using a multi-element standard curve. The Element analysis had a 0.0387 nM limit of detection, and the i-Cap analysis had a limit of detection of 0.71 nM.

**Nutrient and Chlorophyll-*a* Analysis**

Nutrients were filtered using a 0.2 µm syringe filter into a 60 mL bottle frozen at -20 ºC until analysis, and were analyzed in the University of Washington (UW) Marine Chemistry Laboratory with a Seal Analytical AA3 using standard protocols of Gordon et al. (1993).

Chlorophyll-*a* was analyzed shipboard within an hour of CTD collection or incubation end. Standard chlorophyll-*a* protocols were followed with seawater vacuum filtration through 0.7 µm glass-fiber filters (GF/F) on a filtration rack. Chlorophyll-*a* was extracted from the filters using 5 mL of acetone for 24 hours at -20 ℃, following the acetone method (Strickland et al. 1972). After agitation and centrifugation, fluorescence was read on a TD-700 fluorometer (Turner Designs).

Chlorophyll-*a* was converted into a net growth rate, $\mu_{net}$ ($day^{-1}$), in the logarithmic relation shown in *Equation-1*. $Chla_i$ is the initial Chlorophyll-*a* concentration of the treatment group, and $Chla_f$ is the final Chlorophyll-*a* concentration from the respective treatment bottle. Time, t, is in days, related to 2.5 days from the 60-hour incubation period.

**Equation-1**

$$\mu_{net} = \frac{ln(\frac{Chla_f}{Chla_i})}{t}$$

# Results

## Water column characteristics

The CTD cast provided hydrothermal fluid information through ORP from an Eh sensor and beam transmission (Figure 2). At Esmeralda, a minimal response was observed in beam transmission while approaching the summit. A singular ORP peak was observed at 194 m. At NW Rota-1, beam transmission and ORP peaks co-occurred from 385 m to 405 m.

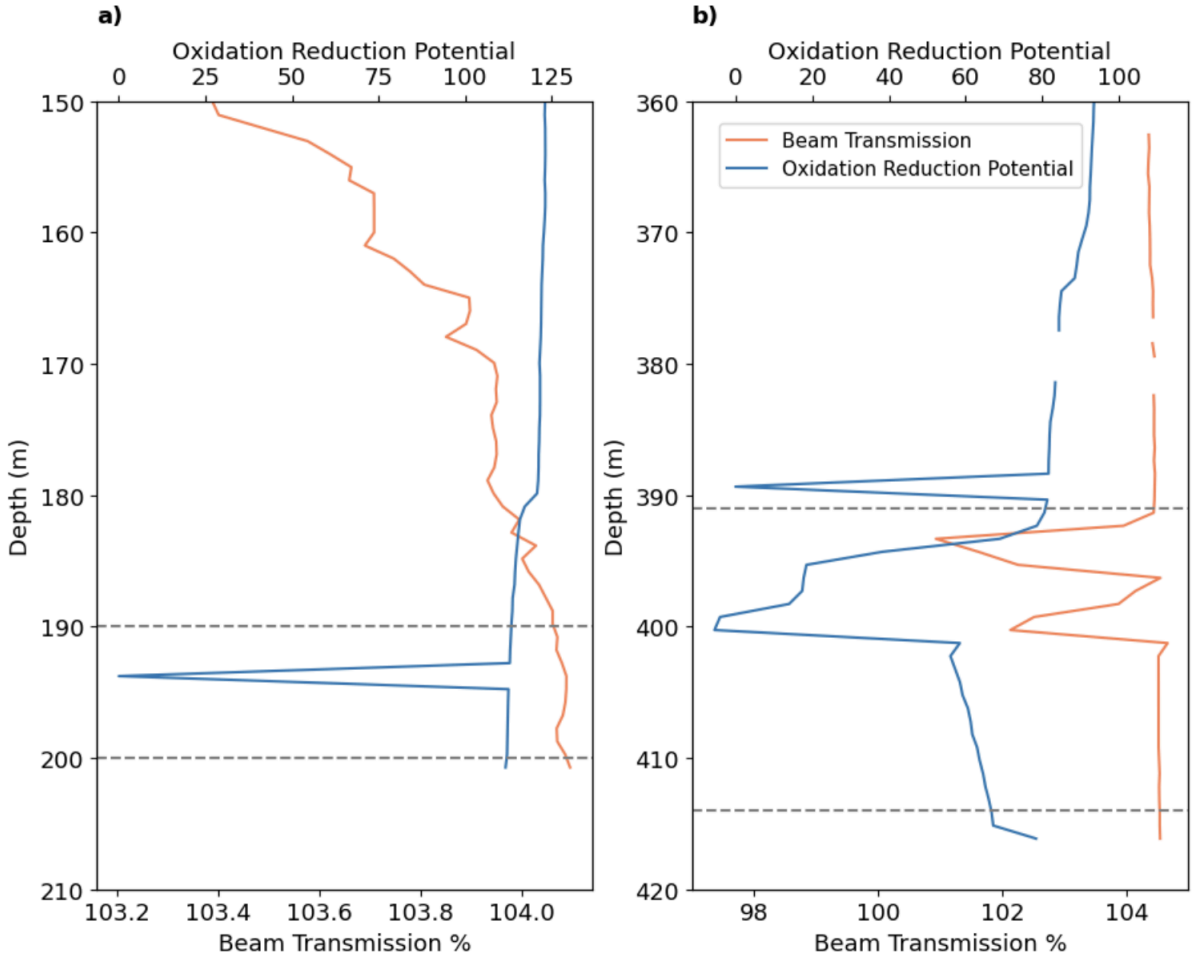


**Figure 2.** Plume indicators at the summits of a) Esmeralda and b) NW Rota-1 seamount, with zoomed-in depth scale to clearly display hydrothermal fluids. The oxidation-reduction potential (blue) is from an Eh sensor (unitless). The beam transmission (orange) detects particles in the water column, with a lower percent representing less transmission and more particles. Co-occurring sharp signal decreases of profiles indicate an increase of suspended particles and reductive fluids, inferred to be hydrothermal plume fluids. Dashed lines represent the depth of spike fluids collected for the respective incubations.

Water column sampling displayed broadly similar nutrient concentrations at the seamount summits compared to the background stations upstream (Figure 3). At all stations, nitrate concentrations ([$NO_3$]) reached a surface minimum at 0 to 8 µM. At approximately 200 m, [$NO_3$] increased, eventually reaching 40 µM at 600 m. Below 600 m, [$NO_3$] was stable between 35 µM and 40 µM (Figure 3).

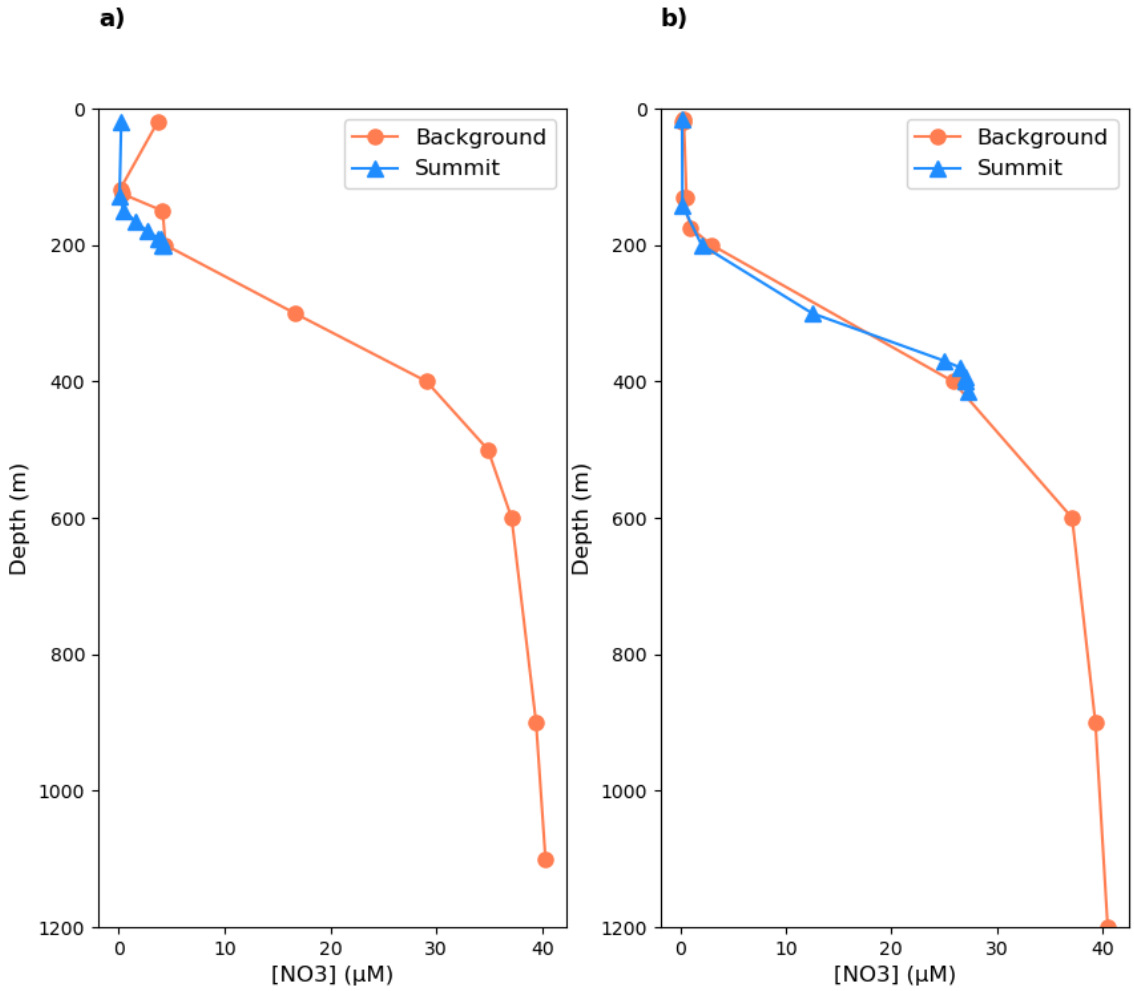


**Figure 3:** Nitrate concentrations at a) Esmeralda and b) NW Rota-1. Each summit (blue, triangle) profile has a comparative background (orange, circle) from 10 nautical miles upstream of the seamount summit.

Phosphate concentrations ([$PO_4$]) were similar between the summit and background stations (Figure 4). [$PO_4$] was low at the surface, maintaining concentrations <0.5 µM. [$PO_4$] increased at 200 m, reaching 1.5 µM at 350 m uniformly across the seamount and background stations. Below 350 m, the NW Rota-1 summit and background stations reached a higher [$PO_4$] maximum of 2.9 µM at depth. Esmeralda reached a maximum [$PO_4$] of 2.0 µM at depth. Both deepwater background stations showed a decrease in [$PO_4$] near the seafloor.

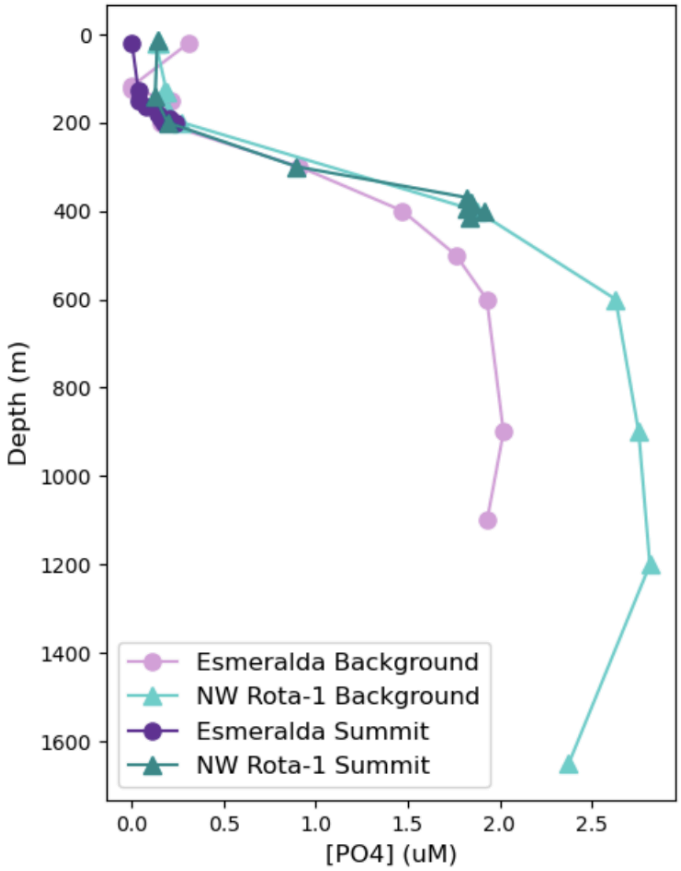


**Figure 4:** Phosphate concentrations at Esmeralda (purple) and NW Rota-1 (teal). Each summit (triangle) profile has a comparative background (circle) from 10 nautical miles upstream of the seamount summit.

Trace metal concentrations were low across the region's surface waters (Figure 5). Increased metal concentrations were observed deeper in the water column, particularly at the seamount summits. NW Rota-1 exhibited lower concentrations with minor peaks reaching <10 nM Fe. At NW Rota-1, there were two Fe peaks at 300 m and 415 m, reaching 4.538±0.091 nM and 4.478±0.090 nM, respectively. Esmeralda, the shallowest seamount, featured multiple peaks, the shallowest at 129 m depth, reaching 24.19±0.484 nM. The highest dissolved Fe concentration was 36.837±0.737 nM at 165 m at Esmerelda. Following this peak and approaching the caldera summit, the dissolved Fe concentration increased again at 180 m to 200 m, reaching 20.936± 0.419nM. Tracey, an inactive seamount in the same region, was used as a reference background for trace metal concentrations. Tracey featured a uniform [Fe] profile with concentrations < 0.9 nM throughout the profile. The summit stations had similar surface [Fe] with Tracey at 0.219±0.012 nM, NW Rota-1 at 0.094±0.010 nM, and Esmeralda at 0.261±0.010 nM.

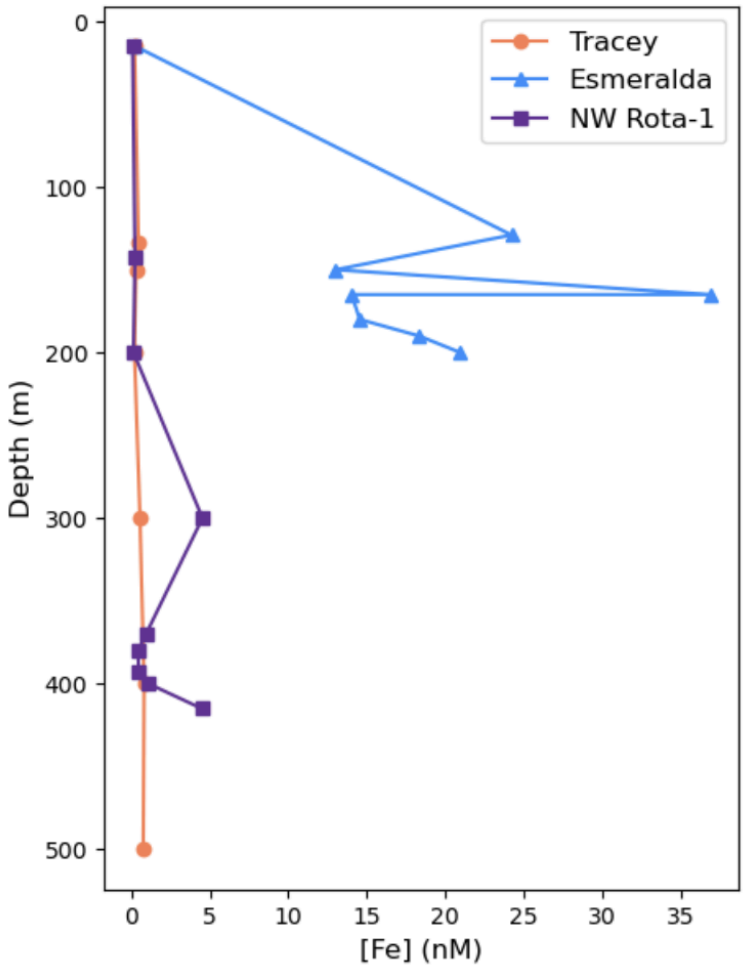


**Figure 5.** Dissolved iron concentrations at seamount summits. Esmeralda (blue, triangle) and NW Rota-1 (purple, square) are hydrothermally active seamounts. Tracey (orange, circle) is hydrothermally inactive and is included as a background reference.

**Phytoplankton growth response in incubation experiments**

In the Esmeralda incubations, growth was observed across all treatments in the 60 hours of incubation (Figure 6). The background treatment with deepwater upstream spike fluids had an average net growth of 0.785±0.053 $day^{-1}$. The caldera treatment had a similar growth response with 0.825±0.042 $day^{-1}$ $\mu_{net}$. The plume net growth response was 0.644±0.030 $day^{-1}$. There was a statistically significant difference in the average $\mu_{net}$ between all of the treatments after 60 hours (one-way ANOVA F = 14.698; *P*-value = 0.00487).

Similarly, in the NW Rota-1 incubations, growth was observed across all treatments in the 60 hours of incubation (Figure 6). The background treatment had the highest average net growth of 0.817±0.020 $day^{-1}$. The caldera had the lowest net growth response at 0.419±0.025 $day^{-1}$. The plume net growth response was 0.668± 0.039 $day^{-1}$. There was a statistical difference in the average $\mu_{net}$ between all of the treatments after 60 hours (one-way ANOVA F = 94.995; *P*-value = 3 x $10^{-5}$).

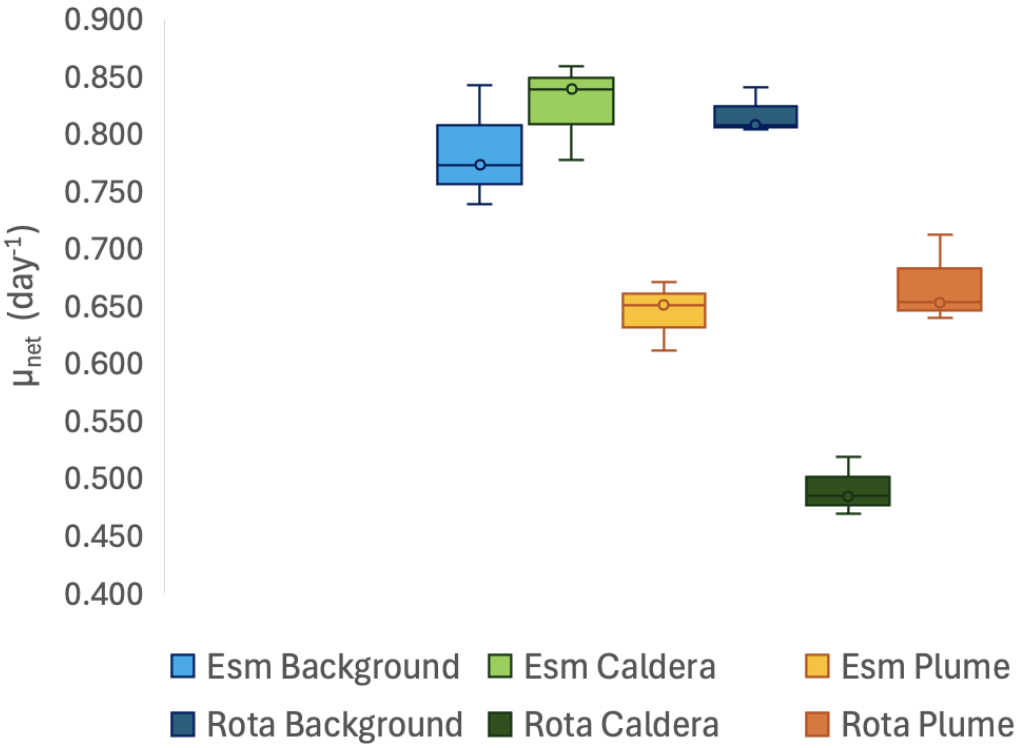


**Figure 6.** Net incubation growth as calculated from *Equation-1* after 60 hours of incubation. The Esmeralda, "Esm", background fluids (light blue) are from 10 nautical miles upstream at 200 m depth. The caldera fluids (light green) are from 200 m, and the plume fluid (yellow) from 190 m. The NW Rota-1, "Rota", background fluids (dark blue) are from 10 nautical miles upstream at 200 m depth. The caldera fluids (dark green) are from 415 m, and the plume (orange) from 393 m. Error bars represent the standard deviation of chlorophyll-*a* measurements from triplicate bottles from each treatment.

Net growth was compared to the uptake of total nitrogen and Fe, as found from the difference between concentrations at the final and initial time points (Figure 7). The smallest growth rate was observed in the NW Rota-1 plume treatment, which also had the least total nitrogen uptake (ΔN), with one treatment bottle showing net nitrogen production over the incubation period. Net growth rates of > 0.6 $day^{-1}$ were seen in all conditions with ΔN > 0.25 μM. The highest net growth rates featured Fe uptake (ΔFe) between 0.5 nM and 2.2 nM. There was no discernible trend in net growth rate with iron uptake.

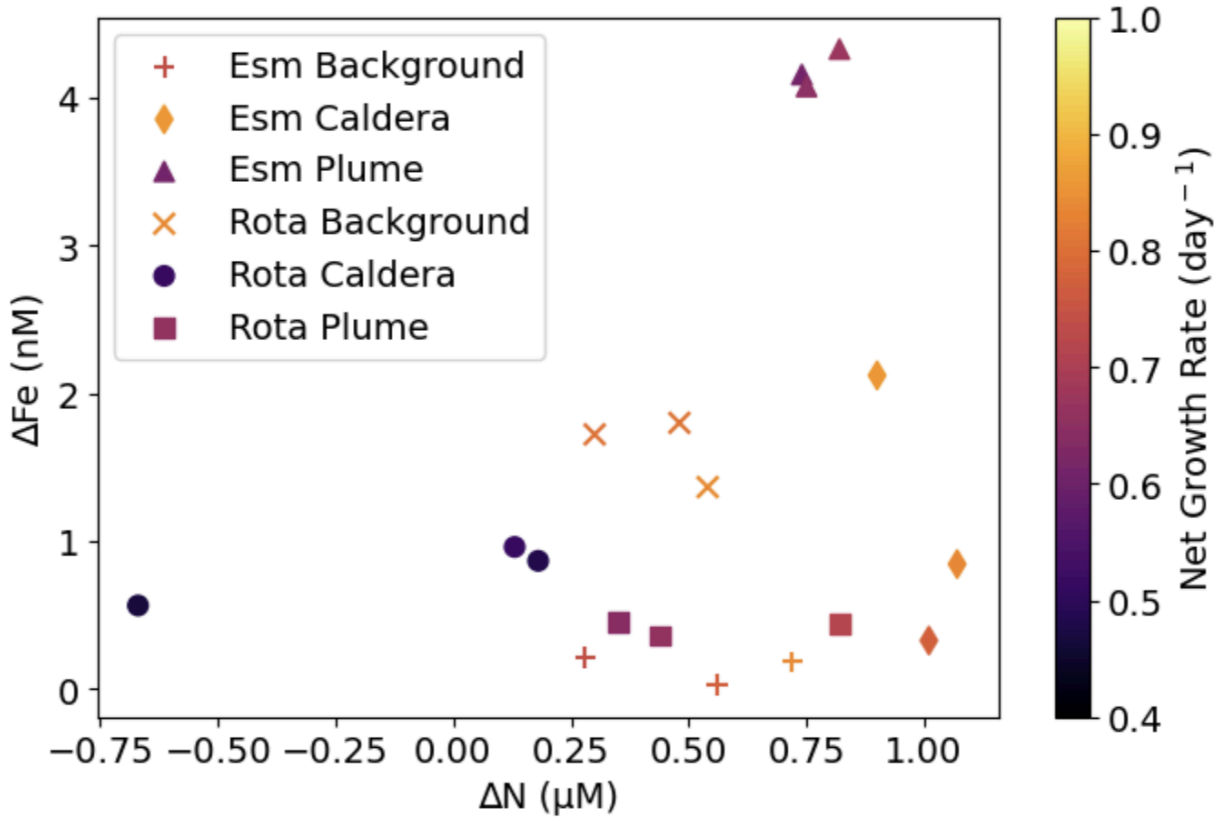


**Figure 7.** Nutrient uptake of dissolvable iron (ΔFe) and nitrogen (ΔN) colormapped with net growth rate. Esmeralda, "Esm" background (+), caldera (diamond), and plume (triangle) incubation results are plotted. NW Rota-1, "Rota" background (X), caldera (circle), and plume (square) incubations are co-plotted on the same color map. Darker purple tones indicate a lower net growth rate, and lighter orange tones indicate a greater growth rate.

To evaluate the impact that micro- and macro-nutrient availability had on growth, the initial [Fe] and total nitrogen [N] were related to the net growth rate (Figure 8). The greatest net growth rate was seen when initial [Fe] was < 4 nM and initial [N] was < 1.5 μM. The greatest net growth was indiscernible in the Esmeralda background, Esmeralda caldera, and NW Rota-1 background treatments with no statistically significant difference (Figure 6).

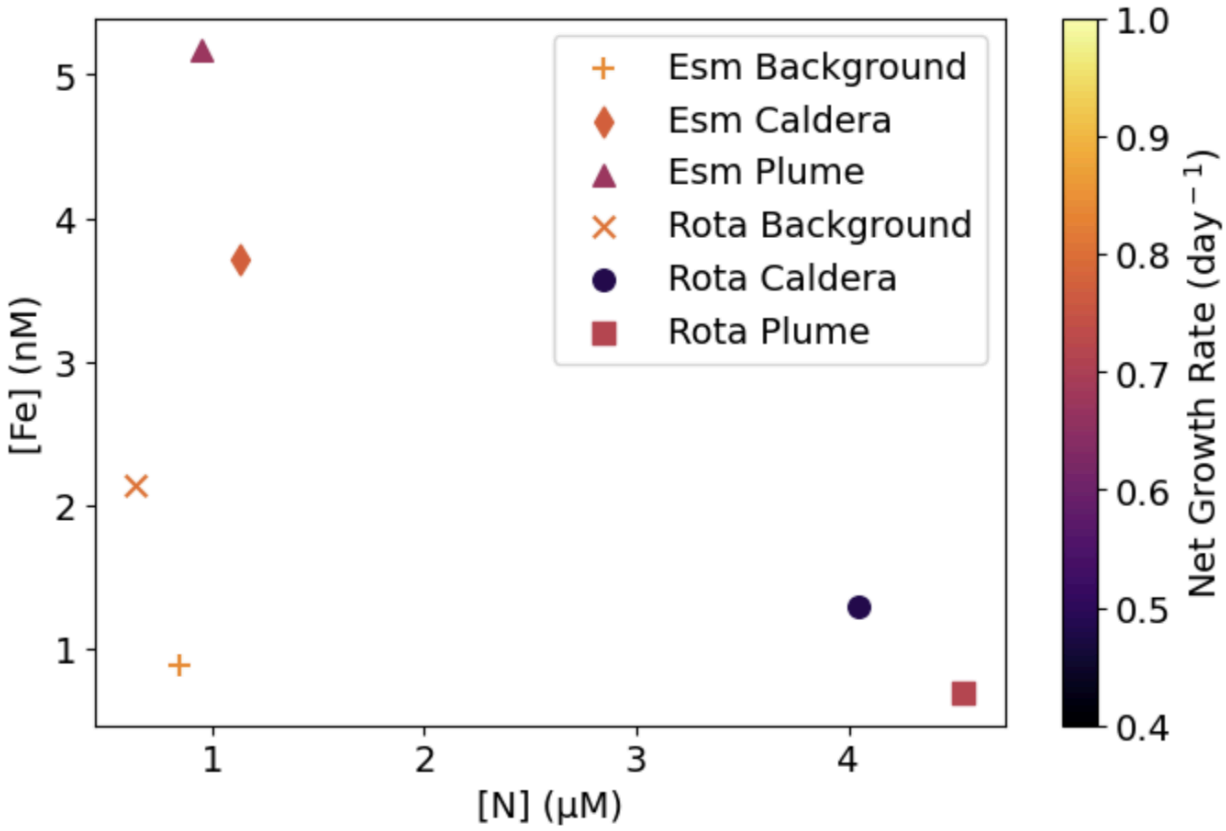


**Figure 8.** Available dissolvable [Fe] and [N] at the start of incubations, colormapped with net growth rate. Emeralda "Esm" treatments include background (+), caldera (diamond), and plume (triangle). NW Rota-1 "Rota" treatments include background (X), caldera (circle), and plume (square). Darker purple tones indicate a lower net growth rate, and lighter orange tones indicate a greater net growth rate.

## Discussion

**Plume signals and incubation source waters**

The clearest plume indicators were seen near NW Rota-1 with a significant decrease in beam transmission, suggesting the presence of particles, and a decrease in the ORP, indicating reductive fluids (Figure 2). These indicators together suggested there were hydrothermal fluids at the summit, specifically between 380 m and 410 m (Figure 5). To capture the response at the top and bottom of the hypothesized plume, incubation spikes were collected from 393 m and 415 m.

At Esmeralda, the beam transmission increases with depth, observed as the lower edge of the deep chlorophyll maximum (DCM), approaching a transmission baseline. This did not provide strong evidence of the presence of hydrothermal activity. The ORP peak at 194 m did indicate the presence of reductive fluids (Figure 2). This informed incubation spike samples to be targeted ~5 m above and below this signal to best capture these fluids, at 190 m and 200 m.

NW Rota-1 and Esmeralda seamounts feature a caldera at their summits, with NW Rota-1 reaching a summit depth of ~470 m and Esmeralda reaching a summit depth of ~250 m. Both seamounts had past reports of hydrothermal activity within their caldera (Resing et al. 2009). This hydrothermalism produces warm fluids that rise and diffuse into the water column, but the caldera prevents some mixing, trapping denser fluids within the rim. This often leads to higher concentrations of metals within the calderas. The plume reaches neutral buoyancy as it cools, creating a second [Fe] maximum slightly shallower in the water column. At Esmeralda, the caldera was seen at 200 m, with two plume peaks at 165 m and 129 m (Figure 5). At NW Rota-1, the caldera fluids were seen at 415 m, and the rising plume at 300 m (Figure 5).

There could be several reasons for the differences in dissolved Fe concentrations between the two seamounts. The [Fe] (Figure 5) and plume indicator (Figure 2) peaks are at similar depths in the water column, but do not exactly coincide. The CTD indicators are limited in time and space by particulate fallout and reactivity; hence, the beam transmission and ORP may not be tightly coupled. This introduces uncertainty as to whether the plume material was accurately captured or if the location was incorrectly interpreted. The ADCP indicated that the prevailing currents were to the northwest, contrary to the expected southwest direction of the region. With a lower rim, NW Rota-1 hydrothermal fluids may have wafted away from the summit. This supports ORP signals seen in CTD casts NW of the summit. As no total particulate Fe samples were taken in this study, there could be differences in the total Fe (dissolved + particulate) at each site, or differences in the ratio between dissolved and particulate (Resing et al. 2009). The multibeam displayed backscatter in the 200 m above the NW Rota-1 summit, indicating particle content, aligned with particle-rich hydrothermal plume waters. Active bubbles were also observed while sampling NW Rota-1 (data not shown), indicating potentially high $CO_2$ or sulfide concentrations at the time of sampling, resulting in scavenging of dissolved Fe. If significant Fe was present at the NW Rota-1 summit, it was not captured in the dissolved form.

The low surface nutrient concentrations are consistent with the nutrient-limited and oligotrophic nature of this region, as noted in past studies (Ma et al., 2019). Nitrate and phosphate profiles at the summit of each seamount very closely follow the trends seen at the respective background stations (Figures 3 and 4). This provides evidence that there is little to no seamount effect on nutrients in this region. There is $< 0.5$ μM variation in $[NO_3]$ and $[PO_4]$ above 450 m between locations, providing consistency across incubations.

Ultimately, similar macronutrient concentrations were present between both seamounts, while Esmerelda had much higher dissolved Fe concentrations despite lower observed hydrothermal activity. The CTD indicators suggest that the plume at Esmeralda may have been older, having more time for particulate material to settle out of the water column and reductive fluids to react. Trapped deeper within the bowl of the caldera, these fluids may be protected from currents with decreased diffusion. This would bridge the low plume indicator response with the high remaining dissolved Fe concentrations.

**Indiscernible incubation growth**

The greatest net growth rates were observed in the Esmeralda and NW Rota-1 background treatments and in the Esmeralda caldera treatment (Figure 6). These net growth rates were not statistically distinct from one another (Tukey's Honestly Significant Difference (HSD) post hoc test; *P*-value > 0.7). In these treatments, the growth effect of adding hydrothermal fluids is not statistically greater than adding non-hydrothermal deep water from the same depth (Figure 6), indicating that the growth was likely induced by general nutrient addition, unspecific to our treatment modalities. The Esmeralda plume treatment had a lower net growth rate than the background and caldera treatments (HSD; *P*-value < 0.005) in both comparisons, despite equivalent nitrogen uptake and greater iron uptake (Figure 7). This suggests that the net growth rate was impacted by more than simply micro- and macro-nutrient uptake in these incubations. This may be a result of the bioavailability of Fe, different phytoplankton species in the treatments, thermal tolerance, or the removal of grazing processes, altering growth controls.

In the NW Rota-1 incubations, the greatest growth was also seen in the background treatment, which had the highest nutrient uptake despite lower initial nutrient availability than the other NW Rota-1 treatments (Figures 7 and 8). There is potential for inclusion of different phytoplankton species in the treatments that would have variable nitrite uptake and growth, complicating the ΔN and ΔFe comparisons. The caldera and plume growth responses at NW Rota-1 were different from each other and different from the NW Rota-1 background (HSD; *P*-value <0.004). The NW Rota-1 caldera treatment had the lowest net growth rate, and net nitrate and phosphate were produced in one triplicate. With high incubation temperatures between 28°C and 30°C, conditions were ideal for bacteria to flourish, potentially remineralizing nutrients (Rivkin and Legendre, 2001). NW Rota-1 is also known to be a highly active and volatile volcano (Resing et al., 2009). The hydrothermal products may have had an inhibitory effect on incubation growth, with a lower pH and high volatiles such as sulfurous acid and carbon dioxide. This suggests that the type of hydrothermalism and the time between the eruption of material and phytoplankton uptake may be key to growth responses.

The net growth rates in the Esmeralda and NW Rota-1 plume treatments were not statistically different from one another (HSD; *P*-Value= 0.960). The Esmeralda treatments had high Fe and low nitrogen, whereas NW Rota-1 treatments had low Fe and high nitrogen (Figure 8). These serve as inverse treatments of nutrient availability and uptake, suggesting Esmeralda was supported by Fe addition and NW Rota-1 by nitrogen addition.

**Integrated effects of hydrothermalism on local productivity**

Esmeralda, the shallowest seamount, did have the greatest dissolved [Fe], reaching the highest in the water column. This shallow seamount venting resulted in elevated [Fe] below the mixed layer and elevated surface production from greater chlorophyll-*a* at time 0. We found that the hydrothermalism at Esmeralda produced more bioavailable Fe, with greater evidence of Fe reaching higher in the water column. This may be the result of the shallower summit, with less diffusion of hydrothermal products. Elevated dissolved Fe approaches the DCM, suggesting that

bioavailable Fe may be traversing into regions of biological productivity. Coupled with increased surface chlorophyll-*a* concentrations at Esmeralda, there is evidence of supplemented surface growth due to hydrothermal outputs, supporting the hypothesis of shallow venting's influence on surface productivity. In contrast, despite high hydrothermal activity, NW Rota-1 may not support primary productivity in the water column. Its lower concentrations of dissolved Fe are deep in the water column and show limited evidence of surface influence. It is concluded that the difference in seamount response is not specific to summit depth, but rather the type and stage of activity, and the form of Fe.

The addition of deep water supported net phytoplankton growth in all treatments, but growth was not found to be strictly dependent on high Fe or $NO_3$. This reinforces that the region is broadly nutrient-limited, and methods of nutrient supplementation could be significant. Iron addition may support nitrogen fixation by diazotrophs, which would in turn supply macronutrients to the region. As Wilson et al. (2019) found, high-temperature geologic processes, like lava flows, can influence surface productivity with localized nutrient supplementation. Even if the geologic inputs of trace metals do not directly impact surface productivity, deep water entrainment of nutrients can be substantial. Similarly, warm hydrothermal fluid may entrain nutrient-rich water at the summit and provide a physical mechanism of transport to bring deep water to the surface. This may be substantial at shallow seamounts where the distance to the euphotic zone remains small.

Hydrothermal nutrient supplementation has supported corresponding phytoplankton blooms in other Fe-limited regions like the Southern Ocean (Schine et al., 2021). With enhanced surface productivity, there is a potential for increased carbon export. Future directions of this research may include the development of a more robust standard sampling and incubation procedure that will help grasp the hydrothermally supplied nutrients' bioavailability. This may include a wider scope of chemical and molecular analyses to evaluate nutrient controls on incubated net growth. More seamounts of a variety of depths and latitudes must be holistically evaluated to draw conclusions on the influence of summit depth on productivity. This research can inform how hydrothermalism may influence primary productivity and better constrain current biogeochemical and climate models.

# Conclusion

Although hydrothermal activity has been well mapped and quantified, few studies have connected hydrothermalism to broader influences on surface productivity. In this study, we describe the influence of Mariana Arc shallow seamounts on primary productivity through water column analysis and incubation experiments. At NW Rota-1 and Esmeralda, each seamount had similar concentrations of macronutrients with significant depletion in the surface layer, suggesting there was not a physical seamount effect on nutrient distribution. All incubations supported net growth, likely due to the deep water supplementation of limiting nutrients. The greatest net growth rate was seen in the background treatments and in the Esmeralda caldera treatment, despite lower initial nutrients and uptake. This suggests that the net growth in this

study may not have been tightly controlled by nitrate and iron as expected, but rather by temperature, community composition, or the presence of volatiles. Esmeralda featured greater dissolved iron concentrations than NW Rota-1, and those elevated concentrations reached higher in the water column. This supports the hypothesis that shallower seamounts have the potential to support greater surface primary production with the summit's proximity to the euphotic zone. Additionally, shallow venting may support a feasible physical mechanism of nutrient delivery through nutrient entrainment in rising plumes. This study remains limited by the unquantified particulate iron and proxies for hydrothermal activity, complicating intercomparison. Further quantification of geologically supplemented nutrients may be significant for refining controls on open ocean primary productivity and influence carbon export and biogeochemical modeling.

## Acknowledgements

I would like to acknowledge and thank the incredible collaborative support that made this project possible. The Captain and crew of the R/V *Thomas G. Thompson*. Randie Bundy for her dedicated mentorship and ongoing support of this project, and the senior thesis instructors for their guidance. The UW Oceanography 444/445 students for their research collaboration and support. The Bundy lab and UW Trace Lab affiliates for their trace metal analysis support. The UW Oceanography community for their ongoing support in furthering students' education and experiences. Figure 1 was a schematic made with BioRender (Created in https://BioRender.com).

# References

Beaulieu, Stace E; Szafrański, Kamil M (2020): InterRidge Global Database of Active Submarine Hydrothermal Vent Fields Version 3.4 [dataset]. PANGAEA, https://doi.org/10.1594/PANGAEA.917894

Buck, N. J., Resing, J. A., Baker, E. T., & Lupton, J. E. (2018). Chemical Fluxes From a Recently Erupted Shallow Submarine Volcano on the Mariana Arc. *Geochemistry, Geophysics, Geosystems*, *19*(5), 1660–1673. https://doi.org/10.1029/2018GC007470.

Kleint, C., Zitoun, R., Neuholz, R., Walter, M., Schnetger, B., Klose, L., Chiswell, S. M., Middag, R., Laan, P., Sander, S. G., & Koschinsky, A. (2022). Trace Metal Dynamics in Shallow Hydrothermal Plumes at the Kermadec Arc. *Frontiers in Marine Science*, *8*, 782734. https://doi.org/10.3389/fmars.2021.782734.

Ma, J., Song, J., Li, X., Wang, Q., Yuan, H., Li, N., & Duan, L. (2021). Analysis of differences in nutrients chemistry in seamount seawaters in the Kocebu and M4 seamounts in Western Pacific Ocean. *Journal of Oceanology and Limnology*, *39*(5), 1662–1674. https://doi.org/10.1007/s00343-020-0239-7.

Ma, J., Song, J., Li, X., Yuan, H., Li, N., Duan, L., & Wang, Q. (2019). Environmental characteristics in three seamount areas of the Tropical Western Pacific Ocean: Focusing on nutrients. *Marine Pollution Bulletin*, *143*, 163–174. https://doi.org/10.1016/j.marpolbul.2019.04.045.

Oliveira, A. P., Coutinho, T. P., Cabeçadas, G., Brogueira, M. J., Coca, J., Ramos, M., Calado, G., & Duarte, P. (2016). Primary production enhancement in a shallow seamount (Gorringe—Northeast Atlantic). *Journal of Marine Systems*, *164*, 13–29. https://doi.org/10.1016/j.jmarsys.2016.07.012.

Resing, J. A., Baker, E. T., Lupton, J. E., Walker, S. L., Butterfield, D. A., Massoth, G. J., & Nakamura, K. (2009). Chemistry of hydrothermal plumes above submarine volcanoes of the Mariana Arc. *Geochemistry, Geophysics, Geosystems*, *10*(2), 2008GC002141. https://doi.org/10.1029/2008GC002141.

Resing, J. A., Sedwick, P. N., German, C. R., Jenkins, W. J., Moffett, J. W., Sohst, B. M., Tagliabue, A. (2015) Basin-scale transport of hydrothermal dissolved metals across the South Pacific Ocean. *Nature*. 2015 Jul 9;523(7559):200-3. doi: 10.1038/nature14577. PMID: 26156374.

Rivkin, R. B., Legendre, L., (2001). Biogenic Carbon Cycling in the Upper Ocean: Effects of Microbial Respiration. *Science* 291,2398-2400. DOI:10.1126/science.291.5512.2398

Schine, C. M. S., Alderkamp, A.-C., Van Dijken, G., Gerringa, L. J. A., Sergi, S., Laan, P., Van Haren, H., Van De Poll, W. H., & Arrigo, K. R. (2021). Massive Southern Ocean phytoplankton bloom fed by iron of possible hydrothermal origin. *Nature Communications*, 12(1), 1211. https://doi.org/10.1038/s41467-021-21339-5.

Strickland, J.D.H., and T.R. Parsons. (1972). A practical handbook of seawater analysis. Fish. Res. Board Can. Bull. 167, 2nd ed. 310 pp.

Tivey, M. (2007). Generation of Seafloor Hydrothermal Vent Fluids and Associated Mineral Deposits. *Oceanography*, 20(1), 50–65. https://doi.org/10.5670/oceanog.2007.80.

UNESCO (1994). Protocols for the joint global ocean flux study (JGOFS) core measurements. Vol. 29.

Wilson, S.T., et al. (2019). Kīlauea lava fuels phytoplankton bloom in the North Pacific Ocean. *Science* 365,1040-1044. DOI:10.1126/science.aax4767

WOCE protocol: Gordon, L. I., J. C. Jennings Jr, A. A. Ross, and J. M. Krest. "A suggested protocol for continuous flow automated analysis of seawater nutrients in the WOCE hydrographic program and the Joint Global Ocean Fluxes Study." Grp. Tech Rpt (1993): 92-1.